ADVANCED MATERIALS
www.advmat.de

Materials Views
www.MaterialsViews.com

Unraveling Unprecedented Charge Carrier Mobility through Structure Property Relationship of Four Isomers of Didodecyl[1]benzothieno[3,2-*b*][1]benzothiophene

Yusuke Tsutsui, Guillaume Schweicher, Basab Chattopadhyay, Tsuneaki Sakurai, Jean-Baptiste Arlin, Christian Ruzié, Almaz Aliev, Artur Ciesielski, Silvia Colella, Alan R. Kennedy, Vincent Lemaur, Yoann Olivier, Rachid Hadji, Lionel Sanguinet, Frédéric Castet, Silvio Osella, Dmytro Dudenko, David Beljonne, Jérôme Cornil, Paolo Samorì, Shu Seki, and Yves H. Geerts**

Since the dawn of organic electronics in the 1970's, academic and industrial research efforts have led to dramatic improvements of the solubility, stability, and electronic properties of organic semiconductors (OSCs).[1,2] The common benchmark to characterize the electrical performances of OSCs is their charge carrier mobility μ ($cm^2\ V^{-1}\ s^{-1}$), defined as the drift velocity of the charge carrier ($cm\ s^{-1}$) per unit of applied electric field ($V\ cm^{-1}$). Reaching high mobilities in OSCs is highly desirable as it allows faster operation of transistors and energy savings by reduced calculation times.[2,3] However, OSCs performances (conventional values usually range from 1 to 10 $cm^2\ V^{-1}\ s^{-1}$, with highest values obtained with single-crystal devices mostly exempt of structural defects) are still not comparable to that of state-of-the-art inorganic semiconductors (e.g., metal oxides with μ = 20–50 $cm^2\ V^{-1}\ s^{-1}$ and polycrystalline silicon with $\mu > 100\ cm^2\ V^{-1}\ s^{-1}$) thereby hampering important potential technological applications such as flexible organic light-emitting diode displays and wearable electronics.[3,4]

Charge carrier mobilities on the order of 50–100 $cm^2\ V^{-1}\ s^{-1}$ at room temperature are conceivable for two reasons: First, a compound as simple as naphthalene exhibits mobilities ranging from 100 to 300 $cm^2\ V^{-1}\ s^{-1}$ between 30 and 3 K;[5] second, recent theoretical calculations prove that there is no reason to believe that achieving mobilities higher than 50 $cm^2\ V^{-1}\ s^{-1}$ is impossible.[6] The highest mobility reported to date, 43 $cm^2\ V^{-1}\ s^{-1}$, has been achieved by Yuan et al. on aligned thin films of a polymorph of 2,7-dioctyl[1]benzothieno[3,2-*b*]-benzothiophene.[7] This value has, however, not been independently reproduced to date.

Charge carrier mobility is a material property depending on multiple parameters among which we can cite molecular and crystalline structures, charge density, temperature, disorder, and defects.[3,8–10] Due to the relative ease of implementation, most of the reported mobility values are extracted from organic field-effect transistor (OFET) characteristics. Hall-effect measurements constitute an alternative robust method that is considerably more difficult to implement.[8,11] Both techniques are contact-based, i.e., implying the injection/collection of charge carriers at electrodes. It is worth mentioning here the recent work of Uemura et al.[12] highlighting how to properly extract without any overestimation the mobility from high-mobility OSCs and the recommendation of Braga et al.[13] Indeed, as

Y. Tsutsui, Dr. T. Sakurai, Prof. S. Seki
Department of Molecular Engineering
Graduate School of Engineering
Kyoto University
Nishikyo-ku, Kyoto 615-8510, Japan
E-mail: seki@moleng.kyoto-u.ac.jp
Dr. G. Schweicher, Dr. B. Chattopadhyay, Dr. J.-B. Arlin, Dr. C. Ruzié, Dr. A. Aliev, Prof. Y. H. Geerts
Laboratoire de Chimie des Polymères
Faculté des Sciences
Université Libre de Bruxelles (ULB)
CP206/1, Boulevard du Triomphe, 1050 Brussels, Belgium
E-mail: ygeerts@ulb.ac.be
Dr. A. Ciesielski, Dr. S. Colella,[+] Prof. P. Samorì
ISIS & icFRC
Université de Strasbourg & CNRS
8 allée Gaspard Monge, 67000 Strasbourg, France
Dr. A. R. Kennedy
Department of Pure and Applied Chemistry
University of Strathclyde
295 Cathedral Street, Glasgow G1 1XL, Scotland
Dr. V. Lemaur, Dr. Y. Olivier, Dr. S. Osella, Dr. D. Dudenko, Dr. D. Beljonne, Dr. J. Cornil
Laboratory for Chemistry of Novel Materials
University of Mons
Place du Parc 20, B-7000 Mons, Belgium
Dr. R. Hadji, Dr. L. Sanguinet
MOLTECH-Anjou UMR CNRS 6200
L'Université Nantes Angers Le Mans (L'UNAM)
Université d'Angers
2 Bd Lavoisier, 49045 Angers Cedex, France
Prof. F. Castet
Institut des Sciences Moléculaires
UMR CNRS 5255
Université de Bordeaux
Cours de la Libération 351, FR-33405 Talence, France
[+]Present address: Dipartimento di Matematica e Fisica "E. De Giorgi", Università del Salento, Via per Arnesano, 73100 Lecce, Italy

DOI: 10.1002/adma.201601285

a result of the possible dependence of the contact resistance with the gate voltage, devices can show a nonlinear drain current swing just above the threshold. It is thus of paramount importance to cross check high mobility values using gated four-point-probe and transmission line method measurements,[8,14] or another measurement method.

The field-induced time-resolved microwave conductivity (FI-TRMC) technique has recently been introduced as a promising approach to avoid contact-related issues.[9] The FI-TRMC technique can not only probe the intrinsic charge carrier mobility at the semiconductor/dielectric interface by microwave-based dielectric loss measurements but also investigate separately hole versus electron conduction by controlling the gate bias voltage. Holding great promises for the rapid screening of a large number of semiconductor/dielectric pairs, this technique has also recently proved its efficiency for quantitative probing of interfacial trap sites.[10,15–17] It must be emphasized that FI-TRMC is complementary to OFET and Hall-effect methods because it probes charge transport over shorter length- and time-scales, allowing thus to investigate the elementary steps of charge transport. FI-TRMC will certainly contribute to elucidate the charge transport mechanism exhibited by weakly van der Waals bonded systems. Indeed, the elaboration of an universal theoretical framework to describe charge transport in OSCs is a challenging task. Until now, extreme models based on a pure hopping regime (in which charges jump from one molecule to another one) or band-like regime (based on the scattering of the charges in delocalized electronic states by lattice phonons) are typically involved in theoretical studies aimed at assessing the influence of various parameters, such as molecular structure, crystalline packing, temperature, and energetic/positional disorder, on transport properties.[3,18] Moreover, as recently highlighted by Fratini et al., the strong dynamical disorder present in OSCs at room temperature imposes a transient localization of the charges which results in an intermediate regime of charge transport where the carriers exhibit both localized and extended characters.[19]

We report here on the structural and electronic properties of four isomers of didodecyl[1]benzothieno[3,2-*b*][1]benzothiophene (C12-BTBT-C12) varying by the isomerism of the alkyl side-chains. The choice of the BTBT core is motivated by the previously reported high mobility values, its high chemical stability, and the ease of derivatization.[7,20–23] FI-TRMC measurements performed on these four derivatives have been confronted to corresponding theoretical simulations in both the hopping and band regime. This work highlights that the molecular packing, driven by the molecular structure of the isomers, has not only a strong impact on the charge carrier mobility but also on the ionization potential (IP) due to changes in the magnitude of electronic delocalization and electronic polarization effects. The FI-TRMC measurements yield a strikingly high average interfacial mobility of 1.7×10^2 cm^2 V^{-1} s^{-1} for 2,7-didodecyl[1]-benzothieno[3,2-*b*][1]benzothiophene. Moreover, the performed simulations point to a band-like transport for this derivative.

The four investigated isomers, whose molecular structures are depicted in **Figure 1**a, exhibit a symmetric conjugated backbone substituted by two dodecyl side chains. As expected, the four compounds exhibit rather comparable first oxidation potentials (E_{ox}^1) around 0.9 eV (vs Fc/Fc^+) in solution with slightly higher values for **1** and **3** than for **2** and **4** (see **Table 1**, Section S2 and Figure S1 of the Supporting Information).[20,24] The thermal behavior of the different BTBTs was investigated by thermogravimetric analysis and differential scanning calorimetry (DSC). Evaporation of the materials occurs at temperatures ranging from 370 to 390 °C (Figure S2a, Supporting Information); DSC traces, as well as transition temperatures and their associated energies, are presented in Figure S2b and Table S1 in the Supporting Information. Almost all the isomers possess only one phase transition except **2** for which a smectic A phase (SmA) is observed prior to melting, as a result of its rod-like molecular shape.[25] With its herringbone motif, the crystal of **2** melts at 117.4 °C. This value is higher than the melting point of the other materials, ranging from 86 to 103 °C. Interestingly, **4** crystallizes in a metastable polymorphic form, upon cooling, which converts into the stable single-crystal phase at 61 °C.

Bulk structure determination of the different BTBT derivatives was realized by single-crystal X-ray diffraction; and the complete crystal data are available in Table S2 in the Supporting Information (the crystal structure of **2** has previously been solved by Takimiya and co-workers).[20,26] Compounds **1–4** exhibit a monoclinic unit cell containing half of the molecule in each asymmetric unit, i.e., $Z' = 0.5$. **2** adopts a standard layer-by-layer herringbone packing motif mainly stabilized by CH$\cdots\pi$ interactions while cofacial interdigitated structures dominated by $\pi\cdots\pi$ interactions are observed for **1**, **3**, and **4** (Figure 1c,d). The shortest stacking distance between molecular planes, 3.48 Å, is obtained for **4;** Table S3 (Supporting Information) highlights the different distances of stacking and slippage exhibited in the structures. **2** presents consequently favorable close contacts between the aromatic cores in two dimensions. Additional information relative to the different structures can be found in Section S4 in the Supporting Information.

The crystal structure of the four isomers being firmly established, we turned our attention to the calculation of the electronic interactions between adjacent π-systems. Table 1 and **Figure 2**a collects the theoretical estimates of two important energetic parameters for charge transport, as calculated from density functional theory (DFT): (i) The transfer integral (J) is involved in both the hopping and band-like models and reflects the degree of electronic overlap/interactions between the interacting electronic levels; Figure 2a also shows the corresponding indexation of the molecules within the bulk single-crystal phase; (ii) the reorganization energy (λ) characterizes the degree of geometric relaxation accompanying the localization of one charge over a single molecule in a hopping picture. For compound **2**, large transfer integrals are calculated for holes along several directions within a molecular layer (from 51 to 58 meV), thus pointing to a 2D charge transport. For all isomers, charge transport cannot be 3D since the transfer integrals between molecules belonging to adjacent layers are close to zero due to the insulating character of the long alkyl chains. In the case of **1**, large transfer integrals (62 meV) are only calculated for dimer 1–2 (along the *a* axis) as a result of the short π-stacking distance, thus leading to a dominant 1D character for the charge transport. The transfer integrals in the other directions are quite small (<6 meV) because the columns of molecules within a layer are shifted parallel and hence do not favor a strong overlap between the highest occupied molecular orbital

ADVANCED MATERIALS
www.advmat.de

www.MaterialsViews.com

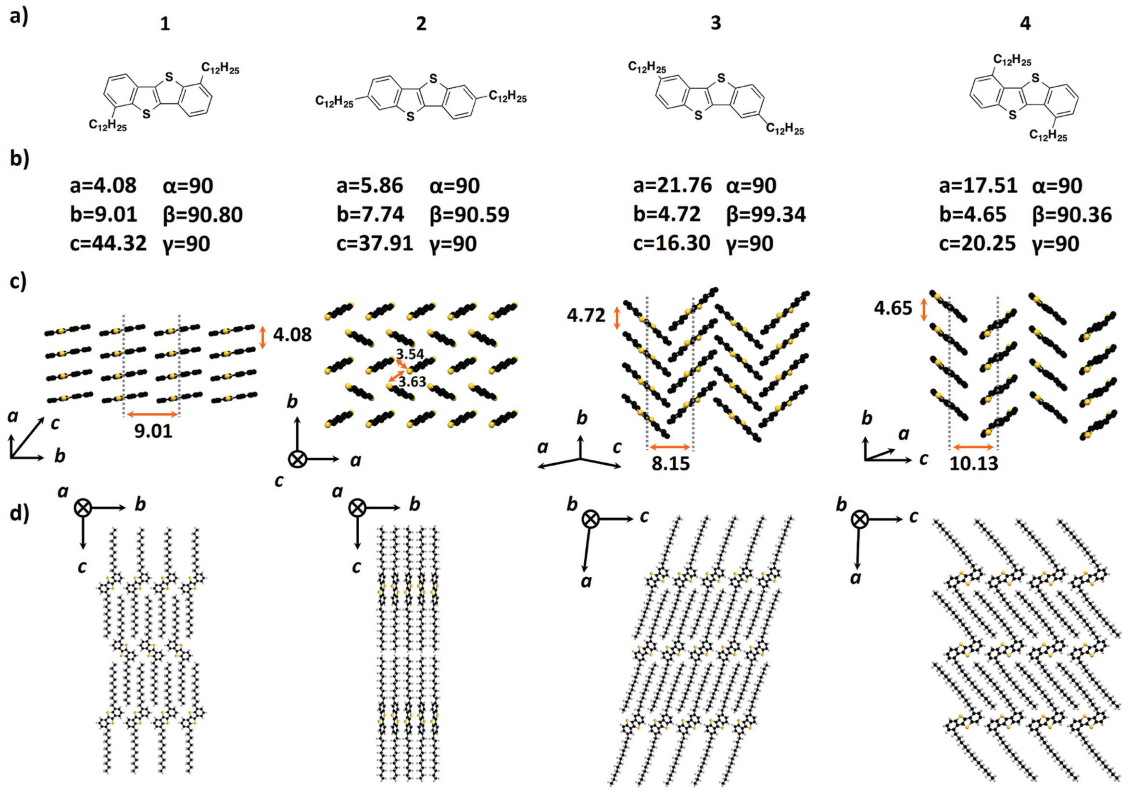

Figure 1. a) Molecular structure of the four isomers of didodecyl[1]benzothieno[3,2-*b*][1]benzothiophene: **1**, **2**, **3**, and **4** presenting substitutions at the 1,6; 2,7; 3,8; 4,9 positions, respectively. b) Lattice parameters of the crystalline structure [Å]. c) Packing of the aromatic cores underscoring the formation of a slipped-stack motif for **1**, classical herringbone motif for **2**, and cofacial herringbone motif for **3** and **4** (*n*-dodecyl chains are omitted for clarity). d) Side view of the packing structure highlighting the side chain behavior.

(HOMO) wave functions. Compounds **3** and **4** adopt a similar packing built from columns of slightly translated molecules (along the *b* direction). However, in contrast to **1**, the molecules between adjacent columns within a layer adopt a herringbone-like arrangement, implying that large spatial overlaps of the HOMO wave functions are possible. This is particularly true for **3** for which significant transfer integrals (15 meV) are estimated within a column but also between adjacent columns within the layers (22 meV). For **4**, very large transfer integrals are also calculated along the π-stacking direction (129 meV) while small values (7 meV) are obtained for hole transfer between adjacent columns, thus reflecting the high sensitivity of the transfer integral values to the relative position of the interacting units.[27] These lower values are primarily attributed to the fact that the long axis of the molecules is almost lying parallel to the organic layer in **4** so that they are only slightly interacting through end-to-end contacts. Altogether, we expect better charge transport properties for **2** in the two regimes owing to its large transfer integrals and its pronounced 2D charge transport character which makes the transport less affected by the orientation of the crystals in the channel of the OFETs. The reorganization energies are very close for the four BTBT structures and range between 0.22 and 0.25 eV for holes, thus suggesting that differences in the charge transport properties among the BTBT derivatives are mainly governed by the amplitude of the transfer integrals in a hopping picture. It is worth mentioning that the calculations have been performed on structures solved at low temperature (except for **2**) and can be affected to a small extent by the thermal expansion and the dynamics of the system.[28]

Table 1. Redox and electronic properties of isomers **1–4**.

Compound	1	2	3	4
E_{ox}^1 [mV]	956	879	950	890
Measured IP - PESA [eV]	5.85	5.27	5.84	5.89
λ_{i+} [eV]	0.22	0.25	0.23	0.22
$\mu^+_{Calc,Max,Hopping}$ [cm^2 V^{-1} s^{-1}]	1.7	3.7	1.6	9.4
$\mu^+_{Calc,Max,Band}$ [cm^2 V^{-1} s^{-1}]	62.5	145.6	8.1	43.9
$(\varphi\Sigma\mu)_{max}$ drop casted [10^{-4} cm^2 V^{-1} s^{-1}]	0.6	14	0.7	1.2
$\mu^+_{FI\text{-}TRMC}$ vapor deposited [cm^2 V^{-1} s^{-1}]	0.2	170	0.1	0.5

Second, we investigated to what extent the electronic properties are impacted by the solid-state packing starting with the ionization potentials. When it is calculated at the Hartree–Fock semi-empirical AM1 (Austin Model 1) level for a single molecule extracted from the crystals, without any further geometry optimization, the variation of IP among the four isomers is less than 50 meV, in good agreement with the small observed variation of E_{ox}^1. However, a radically new picture prevails when molecules interact in the crystals. In sharp contrast with compounds **1**, **3**, and **4**, the isomer **2** exhibits a much lower IP in the solid state. The shift going from the gas phase to the solid state arises from the combination of intermolecular delocalization

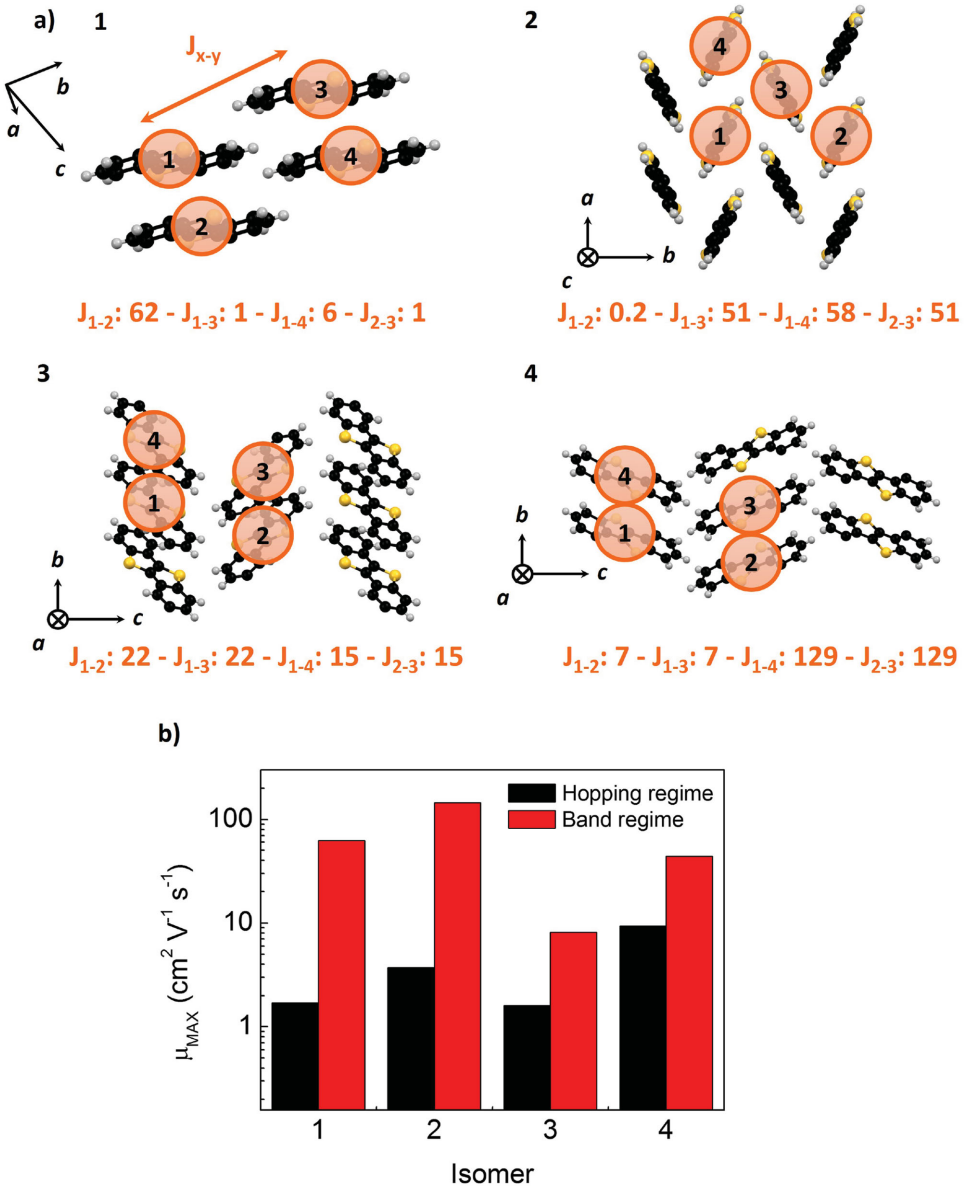

Figure 2. a) Side view of the packing structure of isomers **1**–**4** presenting the indexation of the molecules used for DFT calculations of the transfer integrals (n-dodecyl chains are omitted for clarity) and their related values [meV]. b) Calculated hole mobilities of isomers **1**–**4** in the hopping (black) and band (red) regimes.

effects triggered by the electronic coupling between the molecules and electronic polarization effects driven by electrostatic and induction interactions (see the Experimental Section for details).[29,30] Our theoretical calculations, performed on molecular clusters of similar size, indicate that polarization effects are more pronounced for **2** and lead to a relative change (decrease) of the IP by ≈0.3 eV with respect to the other isomers. Moreover, the additional energy stabilization associated with charge delocalization effects is also more pronounced for **2**, i.e., they contribute to an energy gain of ≈0.3 eV respective to the other isomers, see Table S4 and Figure S5 of the Supporting Information. Altogether, the IP values computed for both the isolated molecules and the crystals are similar for **1**, **3**, and **4**, while **2** shows a 0.6 eV lower IP (Table S4 and Figure S5, Supporting Information). These trends are confirmed byphotoelectron spectroscopy in air (PESA) either on drop casted films or powder samples with values of 5.85, 5.84, and 5.89 eV measured for **1**, **3**, and **4** versus 5.27 eV for **2** (Table 1; Table S5, Supporting Information). To the best of our knowledge, these results provide the first experimental report of an IP variation as large as 0.6 eV among isomers. Note that an increase as large as 1.0 eV in the ionization potential was observed by ultraviolet photoelectron spectroscopy (UPS) going from pentacene to TIPS-pentacene,[31] as further supported by theoretical calculations.[30] Such a result highlights the importance of considering intermolecular interactions in the evaluation of the ionization potential or electron affinity in crystalline films and hence when assessing the ease of charge injection from electrodes.

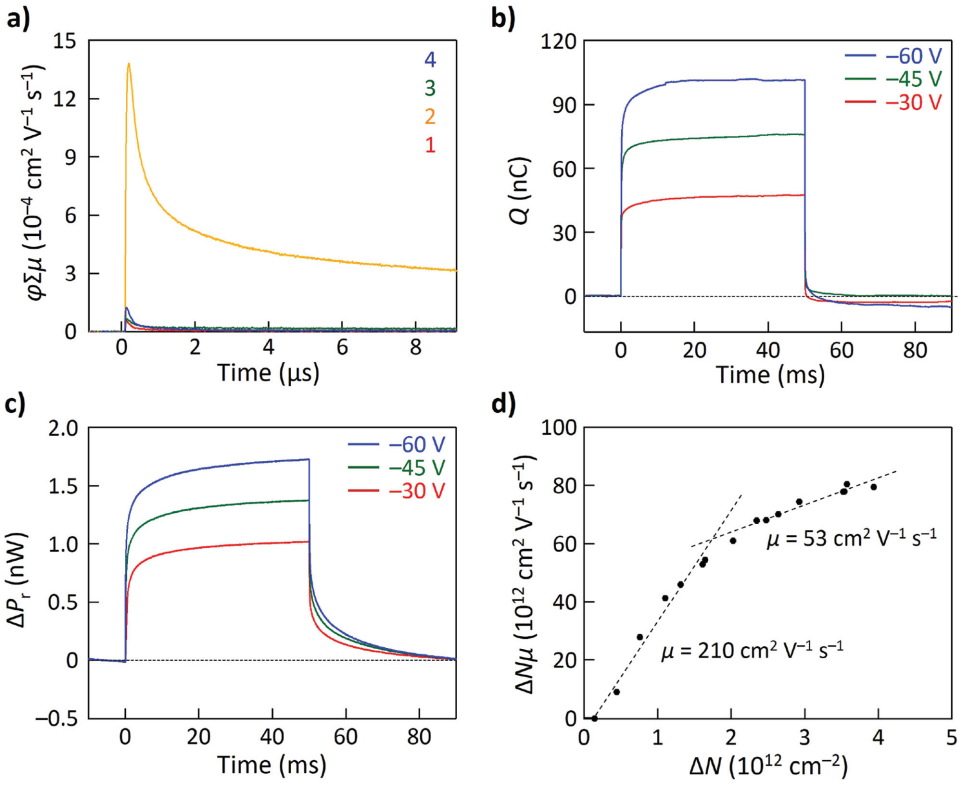

Figure 3. a) FP-TRMC response of the drop casted films of **1**–**4** measured under air. Incident laser intensity and wavelength were adjusted to 5 mW and 355 nm, respectively. b–d) Present the FI-TRMC results obtained on a vapor deposited sample of **2**. Typical time profile of b) the amount of accumulated charge carriers and c) the change in the reflected microwave power in a MIS device of **2**. d) Correlation between the pseudo electrical conductivity $\Delta N\mu$ and the density of injected charge carriers ΔN in a MIS device of **2**. The inset shows the mobility value at low (210 $cm^2\ V^{-1}\ s^{-1}$) and high charge carrier density (53 $cm^2\ V^{-1}\ s^{-1}$).

In order to validate experimentally the peculiar electronic behavior in the solid state of **2**, also reflected by its balanced values of J, charge transport properties of the different isomers were first probed in bulk. The flash-photolysis TRMC (FP-TRMC) technique has proven to be an efficient screening method to address the local-scale intrinsic charge carrier transport properties of OSCs. FP-TRMC is a completely non-contact device-less method where the average lateral motion of charge carriers (parallel to the quartz substrate), photogenerated in the bulk of thin film samples, is monitored through GHz-order microwave spectroscopy (the interested reader can find additional information relative to the FP- and FI-TRMC measurement techniques in the Experimental Section, Figure S6 (Supporting Information) and recent articles and review articles).[10,15,32] As shown in **Figure 3**a, all drop casted films of **1**–**4** gave conductivity transients ($\varphi\Sigma\mu$) with a prompt rise and slow decay upon injection of photogenerated charge carriers (φ and $\Sigma\mu$ represent the quantum yield of generation and sum of the mobilities of positive (μ^+) and negative (μ^-) charge carriers, respectively). Interestingly, **2** provided the highest photoconductivity with a maximum value of $(\varphi\Sigma\mu)_{max} = 1.4 \times 10^{-3}\ cm^2\ V^{-1}\ s^{-1}$. On the other hand, **1**, **3**, and **4** showed photoconductivity of only 0.6, 0.7, and $1.2 \times 10^{-4}\ cm^2\ V^{-1}\ s^{-1}$, respectively. This sharp contrast, over one order of magnitude difference in photoconductivity, is remarkable, although in line with the peculiar behavior of isomer **2**. Specular X-ray diffraction (sXRD) measurements carried on the different samples (drop casted from $CHCl_3$ solutions onto quartz substrates) allowed us to confirm that these results were not impacted by polymorphism or the presence of a preferential molecular alignment (versus the substrate) that could hamper charge transport. Indeed, diffractograms presented in **Figure 4** highlight the presence of highly crystalline thin films, of the single-crystal bulk phase, exhibiting an-edge on preferential alignment of the molecules versus the substrate, favorable for probing the lateral charge transport by FP-TRMC. The situation is slightly more complex in the drop casted films of **4** where two polymorphs are present, mainly the single crystal phase and an unknown thin-film phase that can perturb charge transport. Additional information relatives to the sXRD investigation of the FP-TRMC films can be found in Section S7 in the Supporting Information. The higher $(\varphi\Sigma\mu)_{max}$ value observed for **2** can thus be rationalized by the higher J and dimensionality of its charge transport properties, as a result of its herringbone packing. In contrast, **1**, **3**, and **4**, forming more 1D charge transport pathways, are highly sensitive to the (static) defects and (dynamic) thermal motion of the molecules and lead to lower $(\varphi\Sigma\mu)_{max}$ values.[3,23,33]

Classical mobility measurement in OFETs on polycrystalline thin films (see Section S8 and Figure S9 of the Supporting Information) only confirms the well-established good charge transport properties of **2**, showing an average saturation mobility of 1.6 $cm^2\ V^{-1}\ s^{-1}$.[34] Devices made of **1**, **3**, and **4** were

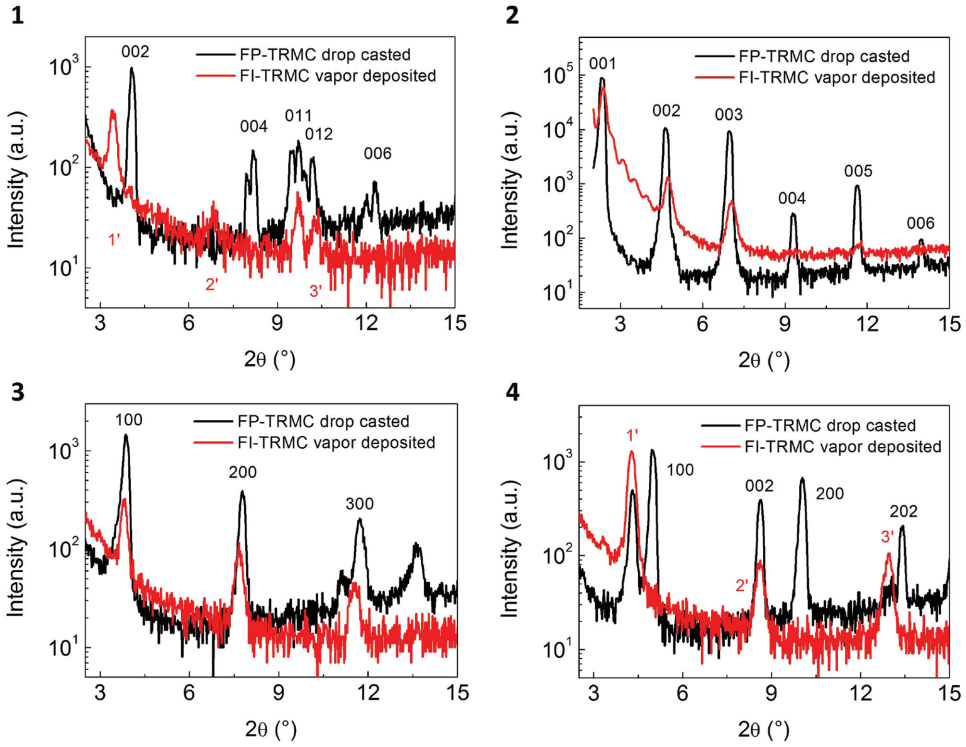

Figure 4. Specular X-ray diffractograms of drop casted and vapor deposited films of **1–4** used for FP- and FI-TRMC measurements, respectively.

strongly impacted by their extremely deep ionization potentials, hampering the injection of charges within the accumulation layer and leading to our inability to record any FET response (either in top or bottom contact configuration).

Since OFETs were not able to corroborate the better charge transport properties of isomer **2**, additional FI-TRMC measurements were performed in metal–insulator–semiconductor (MIS) devices, using SiO_2 and poly(methyl methacrylate) (PMMA) as the dielectric, and vapor deposited films of the different isomers as the active layer (bottom Au/SiO_2/PMMA/OSC/top Au). The vapor deposition of the OSCs is imposed by the FI-TRMC measurement that requires MIS devices presenting smooth surfaces with controlled and reproducible film thicknesses. Holes were injected into the semiconducting layer upon application of a negative voltage and reflected microwave power tracked the accumulated charge carrier density (Figure 3b,c for **2**). Interestingly, the local-scale interfacial hole mobility of **2** was reproducibly estimated as 1.7×10^2 cm^2 V^{-1} s^{-1} (average value for four devices, at charge carrier densities below ≈1.5 10^{12} cm^{-2}) and 2.1×10^2 cm^2 V^{-1} s^{-1} at best (Figure 3d; Figure S10, Supporting Information), considerably higher than any previously reported values on the alkylated BTBT series.[7,21] To the best of our knowledge, this is the first report of an interfacial hole mobility reproducibly exceeding 100 cm^2 V^{-1} s^{-1} in a molecular semiconductor at room temperature. It is worth mentioning again that FI-TRMC measurements allow to probe the lateral charge transport properties of a material (averaged over the area of the MIS device, 0.3 × 0.6 cm^2 = 0.18 cm^2 in our case) at short length- and time-scales (the diffusion length of the charge carriers is estimated by Kubo's equation: $\Delta x = (\mu k_B T f^{-1} e^{-1})^{1/2}$ from several nm up to 150 nm, as a function of the mobility of the investigated OSC and using a microwave frequency f of 9 GHz), i.e., mainly smaller than the dimension of grains giving thus an intrinsic value of the charge mobility. Very interestingly, a second regime of charge transport, exhibiting lower mobility values (25 up to 50% of the value obtained at lower charge carrier density), is observed for charge carrier densities above ≈1.5 10^{12} cm^{-2} (higher voltages, Figure 3d; Figure S10, Supporting Information). Such a decrease in mobility at higher charge carrier density has never been observed before in FI-TRMC measurements. Our previous studies lead to more traditional mobility values, constant up to 6 ×10^{12} cm^{-2}, typically around 4.5 cm^2 V^{-1} s^{-1} for bis[1]benzothieno[2,3-*d*;2′,3′-*d*′]benzo[1,2-*b*;4,5-*b*′]dithiophene (BBTBDT) and up to 6.5 cm^2 V^{-1} s^{-1} for pentacene, the most studied and benchmarked OSC.[10,17] The observation of a drastic difference of mobility at short length- and time-scales on several OSCs and the influence of the charge carrier density for molecular semiconductors exhibiting mobilities higher than 100 cm^2 V^{-1} s^{-1} tend to support the difference of charge transport mechanism taking place in these materials. It is worth noting here that a decrease of mobility has already been observed consistently at room temperature on monolayer graphene and MoS_2 devices upon increase of the charge carrier density, as a result of scattering effects.[35] A similar effect is most probably taking place in our MIS devices of **2** where charges are confined in the first molecular layer at the interface with the dielectric upon applications of voltages higher than ≈7 V (see Section S9 and Figure S11 of the Supporting Information for more details). The use of higher electric fields (higher charge carrier density) certainly make the carriers to get strongly attracted by the interface where they have

to be subjected to scattering effects, as previously reported in rubrene single-crystal OFETs by Takeya et al.[36] Compared to **2**, the other isomers **1**, **3**, and **4** showed a much lower FI-TRMC hole mobility of 0.2, 0.1, and 0.5 $cm^2 V^{-1} s^{-1}$, respectively (Figure S12, Supporting Information). Specular XRD measurements of the films used in the FI-TRMC measurements confirmed that **2** and **3** present their single-crystal phase (Figure 4). The situation is more complex for **1** and **4** exhibiting a mixing between their single-crystal phase and an unknown thin-film phase (presence of 3 correlated peaks) for **1** and only the unknown thin-film phase already observed in the drop casted films for **4** (presence of only one family of correlated peaks). The presence of thin-film phases in the vapor deposited films of **1** and **4** can be attributed to the competition between thermodynamics and kinetics taking place during the nucleation and growth process.[37] Since one of the most salient results of this Communication is the unprecedented charge-carrier mobility of **2** highlighted by the FI-TRMC measurements, we next focus on the theoretical description of the bulk single-crystal phases of the different isomers. Note that a detailed study of the influence of charge carrier density and of the polymorphism in **1** and **4** and its impact on charge transport is currently undergoing and lies outside the scope of this work.

To get a deeper insight into the peculiar behavior of **2** with respect to the other isomers, the hole mobility of all isomers has been computed at the theoretical level in two extreme cases (hopping versus band transport), see the Experimental Section, Table 1 and Section S10 of the Supporting Information. The highest mobilities predicted in a hopping regime are obtained for **4** (9.4 $cm^2 V^{-1} s^{-1}$) and decrease in the order **2**, **1**, and **3** (3.7, 1.7, and 1.6 $cm^2 V^{-1} s^{-1}$, for **2**, **1**, and **3**, respectively). As suggested by the amplitude of the transfer integrals, the mobility anisotropy ratio is the smallest for **2** (see Figure S13 of the Supporting Information).

In the band regime limit, the valence bandwidth spans a range of a few tenths of an eV, from 0.10 eV for isomer **3** up to 0.6 eV for isomer **2** (see Figure S14 of the Supporting Information). The bandwidth of the highest valence band and lowest conduction band along the interlayer direction are strictly zero due to the presence of the alkyl layers. We have computed the hole mobility of all isomers by applying the deformation potential theory coupled to the Boltzmann transport equation. The largest values are obtained for **2** (145.6 and 59.5 $cm^2 V^{-1} s^{-1}$ along the *b* and *a* directions, respectively). **1** and **4** exhibit moderate hole mobilities (62.4 and 4.4 $cm^2 V^{-1} s^{-1}$ for **1** along the *a* and *b* directions and 43.9 $cm^2 V^{-1} s^{-1}$ for **4** along the *b* direction) while the smallest values were found for **3** (6.8 and 8.1 $cm^2 V^{-1} s^{-1}$ along both *b* and *c* directions).

As expected, the hole mobilities calculated within the band regime are larger than those obtained within the hopping regime, though the enhancement factor is significantly larger for **1** and **2** compared to **3** and **4**. Very interestingly, while the measured mobilities compare rather favorably with the hopping values in **1**, **3**, and **4**, the high μ value measured for **2** can only be reproduced by assuming a band regime. This is in line with the expectations that materials with a single dominant transport direction are more strongly perturbed by thermal lattice motions, which break translational symmetry and induce localization of the charge carriers,[19,38] hence validating the use of a hopping picture. In contrast, we speculate that thermal fluctuations have a much more limited impact in the case of compound **2** featuring a pronounced 2D transport. This is corroborated by calculations combining force-field molecular dynamics and electronic structure methods that point to a narrow distribution of the transfer integrals at room temperature in **2** (with a standard deviation of ≈11 meV along the herringbone *a*-direction (dimer 1–4 in Figure 2), to be compared to the corresponding values of 32 and 47 meV in the widely studied pentacene and anthracene molecules, respectively, see Section S10 and Figure S15 of the Supporting Information.[39] Those results are also validated by the recent paper of Illig et al. highlighting the beneficial effect of the alkylation of the aromatic rings along the long axis for BTBT that reduces thermal lattice motions at room temperature and hence hampers its detrimental effect on charge transport properties in OSCs.[40]

As already stated before, FI-TRMC differs mainly from an OFET measurement from the point of view of the charge travelling distance. The former implies that charges travel through roughly 10^5 molecules whereas the latter forces molecules to oscillate only over a few molecules (as a function of the mobility of the investigated OSC, from a few up to 300 molecules in the case of **2**). Such a result, of course, leads to several open questions outside the scope of this initial report. Is the charge really delocalized over a distance of 150 nm or higher for **2**? Will we ever be able to achieve mobilities like these in OFETs? What is the major mechanism hampering charge transport in OSCs?

In summary, the structural and electronic properties of four isomers of didodecyl[1]benzothieno[3,2-*b*][1]benzothiophene have been investigated. Our combined theoretical and experimental study points to the strong impact of the molecular packing on the ionization potential and transfer integrals governing the charge transport. FI-TRMC measurements enabled us to probe the local intrinsic charge carrier transport of those materials, among which 2,7-didodecyl[1]benzothieno[3,2-*b*][1]-benzothiophene was found to exhibit a strikingly high average interfacial mobility of 1.7×10^2 $cm^2 V^{-1} s^{-1}$, at room temperature. Quantum-chemical calculations demonstrate that the transport in **2** operates within the band regime, which we associate with the 2D character of the crystal and the limited thermal fluctuations in electronic transfer integrals. Such a record mobility holds great promise for the field of organic electronics and efforts shall now be invested to further understand how to achieve such high mobilities in contact-based technologies. On the one hand, this will enable a new range of technologies associated to printed OFETs over large areas (flexible displays, wearable computers). On the other hand, it will provide better samples to solid-state physicists and theoreticians to help elucidating the charge transport mechanism that prevails in OSCs, and eventually discover unprecedented physical phenomena.

Supporting Information

Supporting Information is available from the Wiley Online Library or from the author.

Acknowledgements

Y.T. and G.S. contributed equally to this work. The authors acknowledge funding support from the Walloon Region (WCS Project N° 1117306), from the European Commission / Walloon Region (FEDER - Smartfilm RF project), from the Interuniversity Attraction Pole program of the Belgian Federal Science Policy Office (PAI 7/05), from the Programme d'Excellence de la Région Wallonne (OPTI2MAT project), from the Belgian National Fund for Scientific Research (FNRS - Project N° 2.4565.11), from a concerted research action of the French Community of Belgium (ARC Project N° 20061), from a Marie Curie IIF Scheme of the 7th EU Framework Program for the DISCO-project (Grant No. 298319), from a Grant-in-Aid for Scientific Research (Grant Nos. 26620104 and 26102001) by the Japan Society for the Promotion of Science (JSPS), from Shorai Foundation for Science and Technology, from The Murata Science Foundation and the ERC project SUPRAFUNCTION (GA-257305). Y.G. has benefited from a mandate of Francqui Research Professor. G.S. kindly acknowledges postdoctoral fellowship support from the Wiener-Anspach Foundation. P.S. acknowledges also the Agence Nationale de la Recherche through the LabEx CSC (ANR-10-LABX-0026_CSC) and the International Center for Frontier Research in Chemistry (icFRC). D.B. and J.C. are FNRS Research fellows. Crystallographic data for isomer **3** were measured at the DIAMOND light source by the UK National Crystallography Service.

Received: March 6, 2016
Revised: April 10, 2016
Published online: May 25, 2016

[1] a) C. Chiang, C. Fincher Jr., Y. Park, A. Heeger, H. Shirakawa, E. Louis, S. Gau, A. MacDiarmid, *Phys. Rev. Lett.* **1977**, *39*, 1098; b) Y. Olivier, D. Niedzialek, V. Lemaur, W. Pisula, K. Müllen, U. Koldemir, J. R. Reynolds, R. Lazzaroni, J. Cornil, D. Beljonne, *Adv. Mater.* **2014**, *26*, 2119.

[2] H. Sirringhaus, *Adv. Mater.* **2014**, *26*, 1319.

[3] G. Schweicher, Y. Olivier, V. Lemaur, Y. H. Geerts, *Isr. J. Chem.* **2014**, *54*, 595.

[4] a) J. Rivnay, L. H. Jimison, J. E. Northrup, M. F. Toney, R. Noriega, S. Lu, T. J. Marks, A. Facchetti, A. Salleo, *Nat. Mater.* **2009**, *8*, 952; b) V. Podzorov, E. Menard, J. A. Rogers, M. E. Gershenson, *Phys. Rev. Lett.* **2005**, *95*, 226601; c) B. Blülle, R. Häusermann, B. Batlogg, *Phys. Rev. Appl.* **2014**, *1*, 034006.

[5] N. Karl, *Synth. Met.* **2003**, *133*, 649.

[6] a) J. E. Northrup, *Appl. Phys. Lett.* **2011**, *99*, 062111; b) G. Nan, Z. Li, *J. Mater. Chem. C* **2014**, *2*, 1447; c) H. Kobayashi, N. Kobayashi, S. Hosoi, N. Koshitani, D. Murakami, R. Shirasawa, Y. Kudo, D. Hobara, Y. Tokita, M. Itabashi, *J. Chem. Phys.* **2013**, *139*, 014707.

[7] Y. Yuan, G. Giri, A. L. Ayzner, A. P. Zoombelt, S. C. Mannsfeld, J. Chen, D. Nordlund, M. F. Toney, J. Huang, Z. Bao, *Nat. Commun.* **2014**, *5*, 3005.

[8] C. Mitsui, T. Okamoto, M. Yamagishi, J. Tsurumi, K. Yoshimoto, K. Nakahara, J. Soeda, Y. Hirose, H. Sato, A. Yamano, *Adv. Mater.* **2014**, *26*, 4546.

[9] V. Podzorov, *MRS Bull.* **2013**, *38*, 15.

[10] Y. Honsho, T. Miyakai, T. Sakurai, A. Saeki, S. Seki, *Sci. Rep.* **2013**, *3*, 3182.

[11] a) J.-F. Chang, T. Sakanoue, Y. Olivier, T. Uemura, M.-B. Dufourg-Madec, S. G. Yeates, J. Cornil, J. Takeya, A. Troisi, H. Sirringhaus, *Phys. Rev. Lett.* **2011**, *107*, 066601; b) N. A. Minder, S. Ono, Z. Chen, A. Facchetti, A. F. Morpurgo, *Adv. Mater.* **2012**, *24*, 503.

[12] T. Uemura, C. Rolin, T. H. Ke, P. Fesenko, J. Genoe, P. Heremans, J. Takeya, *Adv. Mater.* **2016**, *28*, 151.

[13] D. Braga, G. Horowitz, *Adv. Mater.* **2009**, *21*, 1473.

[14] a) T. Zimmerling, B. Batlogg, *J. Appl. Phys.* **2014**, *115*, 164511; b) T. Okamoto, C. Mitsui, M. Yamagishi, K. Nakahara, J. Soeda, Y. Hirose, K. Miwa, H. Sato, A. Yamano, T. Matsushita, *Adv. Mater.* **2013**, *25*, 6392.

[15] S. Seki, A. Saeki, T. Sakurai, D. Sakamaki, *Phys. Chem. Chem. Phys.* **2014**, *16*, 11093.

[16] W. Choi, T. Miyakai, T. Sakurai, A. Saeki, M. Yokoyama, S. Seki, *Appl. Phys. Lett.* **2014**, *105*, 033302.

[17] Y. Tsutsui, T. Sakurai, S. Minami, K. Hirano, T. Satoh, W. Matsuda, K. Kato, M. Takata, M. Miura, S. Seki, *Phys. Chem. Chem. Phys.* **2015**, *17*, 9624.

[18] a) V. Coropceanu, J. Cornil, D. da Silva Filho, Y. Olivier, R. Silbey, J. Bredas, *Chem. Rev.* **2007**, *107*, 926; b) J. Aragó, A. Troisi, *Adv. Funct. Mater.* **2016**, *26*, 2316.

[19] S. Fratini, D. Mayou, S. Ciuchi, *Adv. Funct. Mater.* **2016**, *26*, 2292.

[20] H. Ebata, T. Izawa, E. Miyazaki, K. Takimiya, M. Ikeda, H. Kuwabara, T. Yui, *J. Am. Chem. Soc.* **2007**, *129*, 15732.

[21] H. Minemawari, T. Yamada, H. Matsui, J. Tsutsumi, S. Haas, R. Chiba, R. Kumai, T. Hasegawa, *Nature* **2011**, *475*, 364.

[22] a) H. Iino, T. Usui, J.-I. Hanna, *Nat. Commun.* **2015**, *6*, 6828; b) K. Takimiya, S. Shinamura, I. Osaka, E. Miyazaki, *Adv. Mater.* **2011**, *23*, 4347; c) K. Takimiya, I. Osaka, T. Mori, M. Nakano, *Acc. Chem. Res.* **2014**, *47*, 1493; d) C. Niebel, Y. Kim, C. Ruzié, J. Karpinska, B. Chattopadhyay, G. Schweicher, A. Richard, V. Lemaur, Y. Olivier, J. Cornil, A. R. Kennedy, Y. Diao, W.-Y. Lee, S. Mannsfeld, Z. Bao, Y. H. Geerts, *J. Mater. Chem. C* **2015**, *3*, 674; e) C. Ruzie, J. Karpinska, A. R. Kennedy, Y. H. Geerts, *J. Org. Chem.* **2013**, *78*, 7741.

[23] G. Schweicher, V. Lemaur, C. Niebel, C. Ruzié, Y. Diao, O. Goto, W.-Y. Lee, Y. Kim, J.-B. Arlin, J. Karpinska, A. R. Kennedy, S. R. Parkin, Y. Olivier, S. C. B. Mannsfeld, J. Cornil, Y. H. Geerts, Z. Bao, *Adv. Mater.* **2015**, *27*, 3066.

[24] a) F. Demanze, J. Cornil, F. Garnier, G. Horowitz, P. Valat, A. Yassar, R. Lazzaroni, J.-L. Bredas, *J. Phys. Chem. B* **1997**, *101*, 4553; b) H. C. Brown, Y. Okamoto, *J. Am. Chem. Soc.* **1958**, *80*, 4979.

[25] J. Leroy, N. Boucher, S. Sergeyev, M. Sferrazza, Y. H. Geerts, *Eur. J. Org. Chem.* **2007**, 1256.

[26] T. Izawa, E. Miyazaki, K. Takimiya, *Adv. Mater.* **2008**, *20*, 3388.

[27] J.-L. Brédas, J. P. Calbert, D. da Silva Filho, J. Cornil, *Proc. Natl. Acad. Sci.* **2002**, *99*, 5804.

[28] a) Y. Li, V. Coropceanu, J.-L. Brédas, *J. Phys. Chem. Lett.* **2012**, *3*, 3325; b) A. S. Eggeman, S. Illig, A. Troisi, H. Sirringhaus, P. A. Midgley, *Nat. Mater.* **2013**, *12*, 1045; c) L. Viani, C. Risko, M. F. Toney, D. W. Breiby, J.-L. Brédas, *ACS Nano* **2014**, *8*, 690.

[29] a) J. Cornil, S. Verlaak, N. Martinelli, A. Mityashin, Y. Olivier, T. Van Regemorter, G. D'Avino, L. Muccioli, C. Zannoni, F. Castet, D. Beljonne, P. Heremans, *Acc. Chem. Res.* **2013**, *46*, 434; b) M. Linares, D. Beljonne, J. Cornil, K. Lancaster, J.-L. Brédas, S. Verlaak, A. Mityashin, P. Heremans, A. Fuchs, C. Lennartz, *J. Phys. Chem. C* **2010**, *114*, 3215; c) F. Castet, P. Aurel, A. Fritsch, L. Ducasse, D. Liotard, M. Linares, J. Cornil, D. Beljonne, *Phys. Rev. B* **2008**, *77*, 115210; d) E. F. Valeev, V. Coropceanu, D. A. da Silva Filho, S. Salman, J.-L. Brédas, *J. Am. Chem. Soc.* **2006**, *128*, 9882.

[30] S. M. Ryno, C. Risko, J.-L. Brédas, *J. Am. Chem. Soc.* **2014**, *136*, 6421.

[31] O. L. Griffith, J. E. Anthony, A. G. Jones, D. L. Lichtenberger, *J. Am. Chem. Soc.* **2010**, *132*, 580.

[32] a) A. Saeki, Y. Koizumi, T. Aida, S. Seki, *Acc. Chem. Res.* **2012**, *45*, 1193; b) A. Saeki, S. Seki, T. Sunagawa, K. Ushida, S. Tagawa, *Philos. Mag.* **2006**, *86*, 1261.

[33] a) J. Tant, Y. H. Geerts, M. Lehmann, V. DeCupere, G. Zucchi, B. W. Laursen, T. Bjornholm, V. Lemaur, V. Marcq, A. Burquel, E. Hennebicq, F. Gardebien, P. Viville, D. Beljonne, R. Lazzaroni, J. Cornil, *J. Phys. Chem. B* **2005**, *109*, 20315; b) Y. Olivier, L. Muccioli, V. Lemaur, Y. Geerts, C. Zannoni, J. Cornil, *J. Phys. Chem. B* **2009**,

113, 14102; c) P. J. Skabara, J. B. Arlin, Y. H. Geerts, *Adv. Mater.* **2013**, *25*, 1948.
[34] S. Colella, C. Ruzié, G. Schweicher, J. B. Arlin, J. Karpinska, Y. Geerts, P. Samorì, *ChemPlusChem* **2014**, *79*, 371.
[35] W. Zhu, V. Perebeinos, M. Freitag, P. Avouris, *Phys. Rev. B* **2009**, *80*, 235402.
[36] J. Takeya, M. Yamagishi, Y. Tominari, R. Hirahara, Y. Nakazawa, T. Nishikawa, T. Kawase, T. Shimoda, S. Ogawa, *Appl. Phys. Lett.* **2007**, *90*, 102120.
[37] A. Virkar, S. Mannsfeld, Z. Bao, N. Stingelin, *Adv. Mater.* **2010**, *22*, 3857.
[38] L. Wang, D. Beljonne, *J. Phys. Chem. Lett.* **2013**, *4*, 1888.
[39] a) A. Troisi, G. Orlandi, *J. Phys. Chem. A* **2006**, *110*, 4065; b) A. Troisi, *Adv. Mater.* **2007**, *19*, 2000.
[40] S. Illig, A. S. Eggeman, A. Troisi, L. Jiang, C. Warwick, M. Nikolka, G. Schweicher, S. G. Yeates, Y. H. Geerts, J. E. Anthony, H. Sirringhaus, *Nat. Commun.* **2016**, *7*, 10736.